Pseudo-CT generation from multiple MR images for small animal irradiation

Shandra Gutierrez Diaz, Roel van Holen, Benedicte Descamps, Nathalie van den Berge, Christian Vanhove

iMinds Medical IT-IBITech, MEDISIP-INFINITY- GROUP ID, Ghent University (UGent), Gent, Oost-Vlaanderen, Belgium

Abstract

Introduction. Computed tomography (CT) is the standard imaging modality for radiation therapy treatment planning (RTTP) because of its ability to provide information on electron density. However, magnetic resonance (MR) imaging provides superior soft tissue contrast, especially in small animal imaging, facilitating the precise selection of the target volume. This makes the technique interesting for irradiation of brain tumors. The aim of this study was to present an MR-only based workflow for RTTP on a small animal radiation research platform (SARRP) by investigating the potential of probabilistic classification of voxels using multiple MR sequences.

Methods. Six female Fisher rats were anesthetized using isoflurane and individually fixed on an in-house made multimodality bed before starting MR and CT acquisitions. MR measurements were performed on a 7-Tesla system using a rat brain volume coil. Four different MR sequences were acquired for each animal, including a T1-weighted (MDEFT) sequence, a T2-weighted (RARE) sequence, an ultra-short echo time sequence with 20 µs echo time (UTE1) and an ultra-short echo time sequence with 2 ms echo time (UTE2). UTE offers the opportunity to acquire images from proton-poor structures with very short transverse relaxation times, such as bone, by using a rapid readout of the fast decaying signal. Following MR, the animals were moved to the SARRP to start a cone-beam CT (CB-CT) by acquiring 720 projections over 360°. Cone-beam CT projection data were reconstructed by filtered back-projection to obtain the standard-CT for RTTP. Then the images were bias field corrected and manually co-registered to the CB-CT. After that, images were segmented in three tissue classes (air, soft tissue and bone) with k-means for the CB-CT and fuzzy c-means segmentation algorithm (FCM) for the MR images with multiple MR images as input. The membership probability can be between 0 and 1, with one indicating 100% probability and zero indicating 0% probability to belong to a specific tissue class. To obtain a pseudo-CT image, voxels were assigned to the tissue class having the highest membership probability. The dice coefficient was used to evaluate the correctness of the segmentation for soft-tissue and bone. The pseudo-CT images with the highest similarity index were used for further radiotherapy treatment planning (RTTP), in addition, to the standard UTE1-UTE2. The target of the RTTP that was selected in the primary cortex (M1) and three different beam arrangements were investigated to compare CB-CT and MR-based dose calculations. The dose plans were a single static beam of 3x3 mm, using a single arc (3x3 mm beam size, 120° arc, couch at 0°), and three non-coplanar arcs (3x3 mm beam size, 120° arc, couch at 0°, 45° and 90°). Dose distributions were calculated using the TPS of the SARRP and cumulative dose volume histograms (DVHs) of the target and normal brain tissue were obtained for the three dose plans.

Results The highest dice coefficient was obtained for the T1-UTE1-T2 combination, which was used for further RTTP. The contribution of bone to the total dice coefficient did not exceed 27%. However, bone accounts for only 2% of the image, therefore a misclassified bone pixel has a bigger effect in the dice coefficient than a misclassified soft tissue pixel. Using only 1 beam, both MR combinations underestimate the dose to be delivered to the target. When more complex beam configurations were used to irradiate the target, very small differences were observed between CB-CT and MR based dose calculations.

Conclusion We presented an MR-only based workflow for RTTP on a small animal radiation research platform that enables both accurate organ delineation and accurate dose calculations using multiple MR contrasts. The proposed method can be very useful when the therapeutic dose has to be delivered in multiple fractions spaced over time, where the cumulative radiation dose of the CT might influence the outcome of a study.

Introduction

For many decades, animal radiation studies were mostly performed using fairly crude experimental setups with radiation fields that did not conform to the target only. Commonly, these experiment were done on devices intended for human patient use and the radiation sources employed were often producing megavoltage (MV) x-rays. MV x-rays have several characteristics that are unsuitable for irradiating small targets in small animals [1]. An MV photon beam exhibits dose build-up at the air–tissue interface in the entrance region of the beam. The extent of this build-up region corresponds roughly to the order of the animal size itself. This makes it very challenging to deliver a uniform dose to a tumor. Another issue is the beam penumbra, which for MV photon beams may extend several millimeters beyond the target, leading to unacceptable dose distributions in small structures. To avoid dose build-up and to obtain extremely sharp penumbras, the use of kilo-voltage (kV) photon beams is required. As a result, efforts were directed towards the development of precise micro-irradiators for small animals [1-3]. These devices are using kV x-ray radiation sources, which combine small animal irradiation with high-resolution cone-beam (CB) computed tomography (CT), as the latter allows accurate beam positioning and dose calculations [4,5]. Although kV-based micro-irradiators have significantly reduced the technological gap between laboratory radiation research and human treatment methods, CB-CT is hampered by extremely low soft-tissue contrast [6] making accurate target selection very difficult. Current research supports the evidence that magnetic resonance (MR) imaging adds valuable information to CT and that it can improve the accuracy of radiotherapy treatment planning (RTTP) [7]. Compared to CT, MR images provide vastly superior soft-tissue contrast, especially in small animal imaging. This makes it much easier to visualize lesion boundaries, which should allow a much better delineation of the target volume, helping to better irradiate the lesion and avoid surrounding tissue. However, MR images cannot be used for dose planning, as they do not provide the required electron density information. As a result co-registration of MR with CT data has become a standard treatment planning procedure in the clinic. Ideally, the complete treatment planning process should rely solely on the information obtained from MR imaging. Using such an MR-only based workflow, the CT acquisitions and the image co-registration process would become redundant. This would significantly reduce the radiation dose to non-target areas, which might become important when delivering the therapeutic dose in multiple fractions spaced over time [8], and the errors associated with the image co-registration process would be avoided.

The aim of this study was to implement an MR-only based workflow for RTTP on a small animal radiation research platform (SARRP) that enables both accurate organ delineation and accurate dose calculations. Pseudo-CT images derived from MR data will be generated to obtain the required electron density

information for dose calculations. To convert MR images into a pseudo-CT scans, the MR volume needs to be segmented into a limited number of tissue classes, and electron density values have to be assigned to these classes to override their default MR values. However, tissue segmentation in MR imaging is far from trivial. Conventional MR sequences provide no signal in lungs and bone, caused by the low proton densities and very short transverse relaxation times of these tissues. As a result, there is no contrast between air, lung and bone. To solve this problem, novel MR sequences have been implemented that acquire the MR signal directly after radio-frequency excitation, such as the ultra-short echo time sequence (UTE). The extra information provided by this sequence can be used to facilitate the conversion of MR images into a pseudo-CT [9,10]. We will investigate the potential of probabilistic classification of voxels by acquiring multiple MR sequences [11]. To our knowledge, this is the first study that investigates the use of an MR-only based workflow in pre-clinical RTTP.

Material and Methods

Animals

All animals were treated according to guidelines approved by the European Ethics Committee (2010/63/EC) and approved by the Animal Ethical Committee of Ghent University (ECD 12/28-A1). Six adult female Fisher rats (weight 174±7g) were purchased from Charles River (Neder-over-Heembeek, Belgium). The animals were kept under environmentally controlled conditions (12h normal light/dark cycles, 20-23°C and 50% relative humidity) with food and water ad libitum.

During the imaging experiment, animals were anesthetized with 2% isoflurane mixed with medical oxygen (0.3 L/min).

Image acquisition

Rats were positioned on an in-house made multimodality bed to facilitate animal transport from the MR to the small animal irradiator. MR images of the rat brain were acquired on a 7 T PharmaScan MR system (Bruker, Ettlingen, Germany) using a 40 mm Bruker quadrature volume transmit/receive radiofrequency coil. Four different MR sequences were acquired, including a T1-weighted MDEFT sequence (TR/TE/TI = 1700/3.5/1100 ms, FA = 20°, NA = 1, TA = 29 min, voxel size = 275x500x275µm, 1283 matrix), a T2-weighted RARE sequence (TR/TE = 16000/37ms, FA= 164.4°, NA = 3, TA = 12 min, voxel size = 275x500x275µm, 1283 matrix), an ultra-short echo time sequence with 20 µs echo time (UTE1) (TR/TE = 8/0.02ms, FA= 7.5°, NA = 3, TA = 20 min, voxel size = 275x500x275µm, 1283 matrix) and an ultra- short echo time sequence with 2 ms echo time (UTE2) (TR/TE = 8/2ms, FA= 7.5°, NA = 3, TA = 20 min, voxel size = 275x500x275µm, 1283 matrix). All MR images were acquired in the coronal orientation.

Immediately after the MR acquisitions, the animals were moved to the SARRP

(XStrahl, Surrey, UK). A CB-CT scan was acquired with the exposure settings set to 70 kV, 1mA, 720 projections, 360° rotation and 1 mm aluminum filtration. The acquired CB-CT projection data were reconstructed using a modified Feldkamp reconstruction algorithm to a cubic voxel size of 0.275 mm into a 411x251x411 matrix.

Image processing

MR images were bias field corrected [12] and manually co-registered to the reconstructed CB-CT by rigid body transformations using anatomical landmarks. The reconstructed CB-CT images were automatically segmented into three tissue classes (air, soft tissue and bone) using a k-means clustering algorithm [13]. These segmented CB-CT images were used as a reference for further dose calculations using the treatment planning software (TPS) of the SARRP (3DSlicer version 3.6.3).

To classify air, soft tissue and bone on the MR images, the images were automatically segmented into three tissue classes using the fuzzy c-means segmentation algorithm (FCM) [14] with multiple MR images as input. The FCM algorithm assigns voxels a probability to belong to a specific tissue class. The membership probability can be between 0 and 1, with one indicating 100% probability and zero indicating 0% probability to belong to a specific tissue class. When segmentation is done into three tissue classes, the sum of the probabilities to belong to one of the three tissue classes is 1. To obtain a pseudo-CT image, voxels were assigned to the tissue class having the highest membership probability.

All possible combinations of the four MR images were used as input to the FCM algorithm, resulting in 15 different pseudo-CT images. The similarity between segmented CB-CT and pseudo-CT images was evaluated by using the dice coefficient [15]:

$$Dt = \frac{2|CTt \cap MRt|}{|CTt| + |MRt|}$$

where CTt and MRt represent the voxels classified as tissue class t in the segmented CB-CT pseudo-CT images, respectively. The dice coefficient can be between 0 and 1; with one indicating identical segmentation for tissue class t. The dice coefficient was calculated for bone and soft tissue. The sum of both coefficients was calculated as the final measure for similarity.

The pseudo-CT images with the highest similarity index were used for further RTTP.

Radiotherapy treatment planning

Segmented CB-CT, pseudo-CT and T2-weighted MR images were imported in the TPS of the SARRP. The T2-weighted images were used to select the target of the

RTTP that was chosen to be in the primary cortex (M1). Different beam arrangements were investigated to compare CB-CT and MR-based dose calculations. Three different dose plans were calculated to deliver 15 Gy to the target: using a single static beam of 3x3 mm, using a single arc (3x3 mm beam size, 120° arc, couch at 0°), and three non-coplanar arcs (3x3 mm beam size, 120° arc, couch at 0°, 45° and 90°). Dose distributions were calculated using the TPS of the SARRP and cumulative dose volume histograms (DVHs) of the target and normal brain tissue were obtained for the three dose plans.

Results & Discussion

Similarity index

Figure 1 shows the similarity between the segmented CB-CT and the 15 pseudo-CT images obtained by using the 15 possible combinations of the four MR images as input to the FCM algorithm. The highest dice coefficient was obtained for the T1-UTE1-T2 combination, which was used for further RTTP. In addition, dose calculations were also done for the UTE1-UTE2 combination that is commonly used to provide CT information from MR images [9,10].

As noted by other investigators [11] our results also indicate that UTE2 does not add valuable information to the segmentation process.

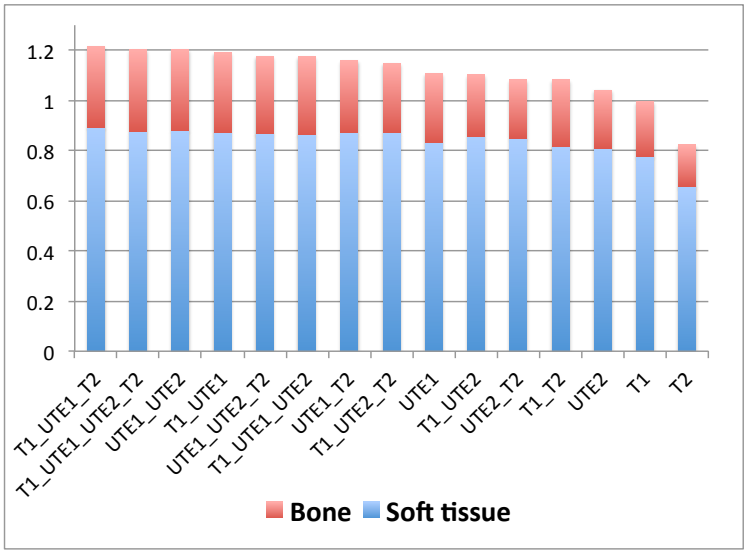

Figure 1. Total dice coefficient of combination of MR images for bone (in red) and soft tissue (in blue) segmentation.

The contribution of bone to the total dice coefficient did not exceed 27%. This is related to the short repetition time necessary for a UTE sequence, resulting in loss of signal observed in tissues with long T1, such as the vitreous body in the eyes. Consequently, the eyes are misclassified as bone when UTE images are used during the segmentation process (see Figure 2). However, the eyes are sensitive to irradiation and can be considered as organs at risk during treatment planning. In addition, bone accounts for only 2% of the image, therefore a misclassified bone pixel has a bigger effect in the dice coefficient than a misclassified soft tissue pixel.

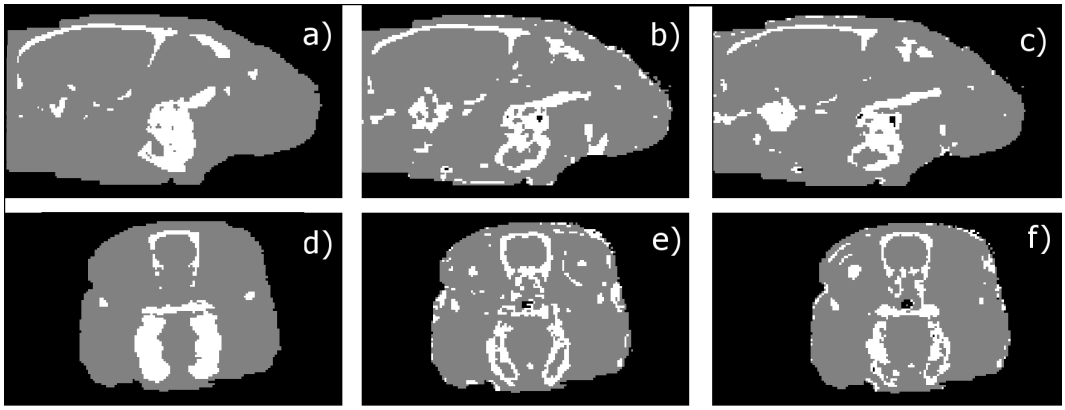

Figure 2. Segmented images in three tissue classes; air (black), bone (white) and soft tissue (gray). Coronal and sagittal view of CT (a,d), UTE1-UTE2(b,e) and T1-UTE1-T2(c,f) respectively.

Dose volume histograms

Figure 3 displays the DVHs in the target volume and the normal brain for CB-CT and two MR-based dose calculations. Results are shown for the three beam arrangements.

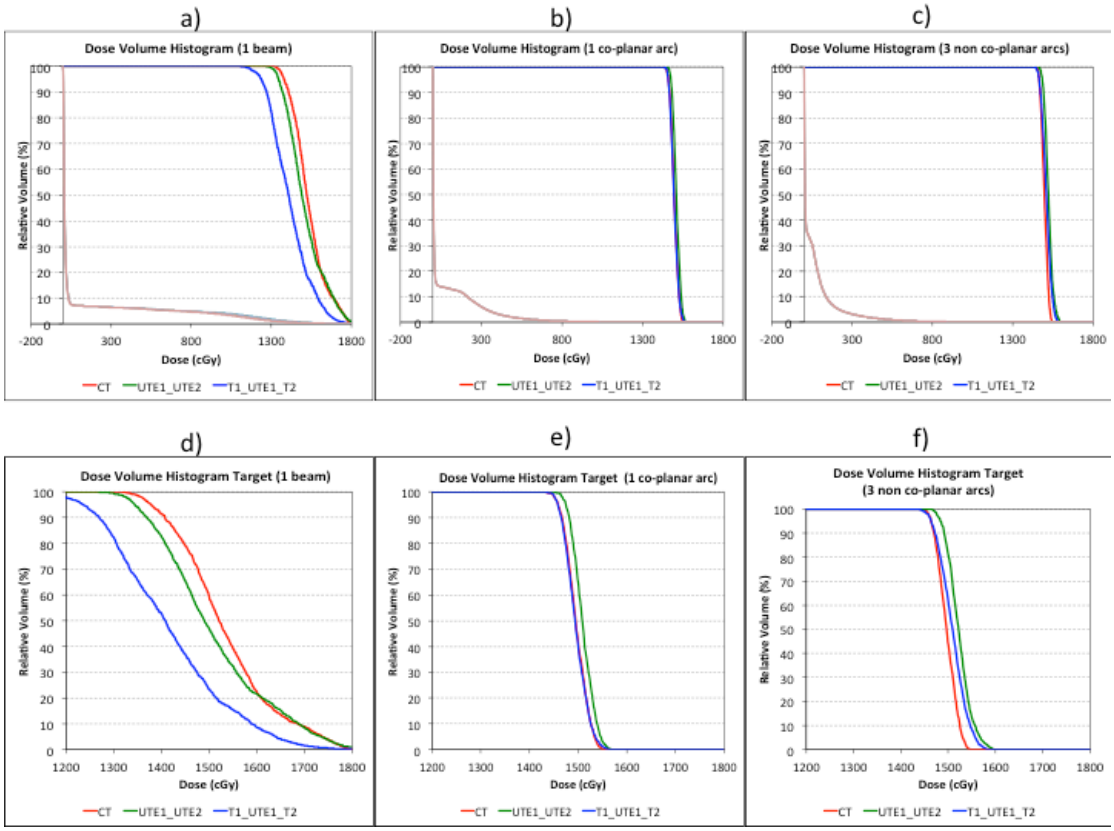

Figure 3. DVH in the target and in the brain of CT (red), UTE1-UTE2 (green) and T1-UTE1-T2 (blue) with (a) 1beam, (b) 1 co-planar arc and (c) 3 non-coplanar. (d)-(f) Amplification of the above DVH in the target.

Using only 1 beam, both MR combinations underestimate the dose to be delivered to the target. Figure 3a and 3d show that the UTE1-UTE2 combination outperforms the T1-UTE1-T2 combination. However, this result cannot be

generalized for every beam, because changing the beam position will also change the DVHs.

When more complex beam configurations were used to irradiate the target (more similar to the clinic), very small differences were observed between CB-CT and MR based dose calculations (Figure 3b, 3c, 3e and 3f) and the results are more in agreement with the dice coefficient. In contrast to some reports in literature [11, 16] the doses that have to be delivered to the target were slightly overestimated when the pseudo-CT images were used during RTTP. The most likely explanation is that parts of the air cavities in the rat head can be misclassified as bone, increasing the dose to the target when MR-based dose calculations are performed.

For future work, we will study the bone segmentation improvement by applying other segmentation algorithms such as graph cuts.

Conclusion

We presented an MR-only based workflow for RTTP on a small animal radiation research platform that enables both accurate organ delineation and accurate dose calculations using multiple MR contrasts. The proposed method can be very useful when the therapeutic dose has to be delivered in multiple fractions spaced over time, where the cumulative radiation dose of the CB-CT might influence the outcome of a study.

References

1. Verhaegen F, Granton P, Tryggestad E. Small animal radiotherapy research platforms. Phys Med Biol. 2011;56:R55–R83.
2. Wong J, Armour E, Kazanzides P, Iordachita I, Tryggestad E, Deng H, Matinfar M, Kennedy C, Liu Z, Chan T, Gray O, Verhaegen F, McNutt T, Ford E, DeWeese TL. High-resolution, small animal radiation research platform with x-ray tomographic guidance capabilities. Int J Radiation Oncology Biol Phys. 2008;71:1591–99.
3. Matinfar M, Iyer S, Ford E, Wong J, Kazanzides P. Image guided complex dose delivery for small animal radiotherapy. IEEE Proceeding International Symposium on Biomedical Imaging: From Nano to Macro;2009:1243-46.
4. Aird E, Conway J. CT Simulation for radiotherapy treatment planning. Br J Radiol. 2002;75:937–49.
5. Baker GR. Localization: conventional and CT simulation. Br J Radiol. 2006;79:S36-S49.
6. Siewerdsen JH, Moseley DJ, Bakhtiar B, Richard S, Jaffray DA. The influence of antiscatter grids on soft-tissue detectability in cone-beam computed tomography with flat-panel detectors. Med Phys. 2004;31:3506-20.
7. Divya Shukla, Nagraj G. Huilgol, Naresh Trivedi et al. T2 weighted MRI in assessment of volume changes during radiotherapy of high grade gliomas. J Cancer Res Ther. (2005): 235-238.
8. Said Daibes Figueroa, Christopher T. Winkelmann, William H. Miller et al.

"TLD assessment of mouse dosimetry during microCT imaging TLD assesment of mouse dosimetry during microCT imaging." Med Phys. (2008): 3866-3874.
9. Keereman V, Fierens Y, Broux T, De Deene Y, Lonneux M, Vandenberghe S. MRI-Based Attenuation Correction for PET/MRI Using Ultrashort Echo Time Sequences J Nucl Med. 2010;51:812–8.
10. Keereman V, Fierens Y, Vanhove C, Lahoutte T, Vandenberghe S. MR-based attenuation correction for micro-SPECT. Mol Imaging. 2012;11:155-65.
11. Hsu SH, Cao Y, Huang K, Feng M, Balter JM. Investigation of a method for generating synthetic CT models from MRI scans of the head and neck for radiation therapy. Med Phys. 2013;58:8419-8435.
12. Chunming Li, Chenyang Xu, Adam W, Anderson et al. MRI Tissue Classification and Bias Field Estimation Based on Coherent Local Intensity Clustering : A Unified Enery Minimization Framework. Inf Process Med Imaging 21 (2009): 288-99.
13. Hartigan, J. A.; Wong, M. A. (1979). Algorithm AS 136: A K-Means Clustering Algorithm. Journal of the Royal Statistical Society, Series C 28 (1): 100–108.
14. Bezdek, James C. (1981). Pattern Recognition with Fuzzy Objective Function Algorithms. ISBN 0-306-40671-3.
15. Sørensen, T. (1948). A method of establishing groups of equal amplitude in plant sociology based on similarity of species and its application to analyses of the vegetation on Danish commons. Kongelige Danske Videnskabernes Selskab 5 (4): 1–34.
16. Lambert J., Greer P.B.,Menk F., Patterson J., Perker J. et al. MRI-guided prostate radiation therapy planning: Investigation of dosimetric accuracy of MRI-based dose planning. Radiother Oncol.2011; 330-334.